



# Zinc doping of different nanoparticles of TiO<sub>2</sub> Sachtopore for improved elimination of the methyl orange by photocatalysis

Boutaina Regraguy<sup>1</sup> · Imane Ellouzi<sup>1</sup> · Jamal Mabrouki<sup>1</sup> · Maryem Rahmani<sup>1</sup> · Fatine Drhimer<sup>1</sup> · Chaimaa Mahmoud<sup>1</sup> · Abdelmalek Dahchour<sup>2</sup> · Mohammadine El Mrabet<sup>2</sup> · Souad El Hajjaji<sup>1</sup>

Received: 10 May 2022 / Accepted: 31 July 2022 / Published online: 12 August 2022  
© Qatar University and Springer Nature Switzerland AG 2022

## Abstract

Heterogeneous photocatalysis is an increasingly popular method used to decontaminate polluted water. Dyes have become one of the major sources of water pollution and methyl orange is one of the most commonly used dyes in the textile industries. The objective of this study was to remove MO and compare the efficiency of the synthesized photocatalysts. In the current work, photodegradation of methyl orange dye, selected as a pollutant model is carried out at room temperature in aqueous solution of Zn-doped TiO<sub>2</sub>. The photocatalysts tested in this study were prepared by coprecipitation method. The catalysts were characterized by XRD, TEM, SEM, EDS, and DRS, before proceeding to photodegradation. X-ray diffraction showed that samples are only composed of TiO<sub>2</sub> anatase, except TiO<sub>2</sub> P25, which contains some crystallites in the rutile form. According to TEM, all nanoparticles of the different photocatalysts have a spherical, clearly dispersed and fine morphology. A strong agglomeration is observed for TiO<sub>2</sub> P25. Energy dispersive X-ray spectroscopy confirmed Zn doping by the presence of peaks attributed to zinc. The UV–Vis diffuse reflectance spectroscopy (UV–Vis DRS) shows a shift of absorption from the UV region to the visible light region and shows that all nanoparticles have very similar absorption thresholds, thus the doped catalysts are promising materials for the use of visible light. The obtained results during the study of the adsorption showed that the order of adsorbability varies in the following decreasing direction: TiO<sub>2</sub> Sachtopore (ZnCl<sub>2</sub>/TiO<sub>2</sub> = 0.2%) > TiO<sub>2</sub> Sachtopore (ZnCl<sub>2</sub>/TiO<sub>2</sub> = 0.1%) > pure TiO<sub>2</sub> Sachtopore > TiO<sub>2</sub> P25. The photodegradation kinetics was studied as a function of several parameters. A comparison of the degradation kinetics of methyl orange has shown that TiO<sub>2</sub> P25 provides comparable performances to doped TiO<sub>2</sub> Sachtopore at 0.2% of Zn. 1 g/L is the optimum concentration for all catalysts used. The synthesized nanomaterials showed good photodegradation ability in MO decomposition, as well as the results reveal that photocatalysis is a very suitable technique for the purification of water containing methyl orange.

## Highlights

- Compared to other photocatalysts, doped TiO<sub>2</sub> Sachtopore (ZnCl<sub>2</sub>/TiO<sub>2</sub> = 0.2%) has a higher adsorption capacity.
- 1 g/L is the optimum concentration for all samples used during this study.
- 0.2% of zinc reveals significant results than other percentages.

**Keywords** Adsorption · Photodegradation · Methyl orange · ZnCl<sub>2</sub>/TiO<sub>2</sub> · Water treatment

✉ Jamal Mabrouki  
j.mabrouki@um5r.ac.ma

Souad El Hajjaji  
s.elhajjaji@um5r.ac.ma

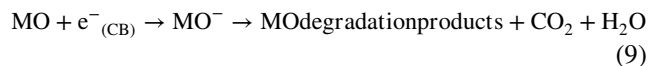
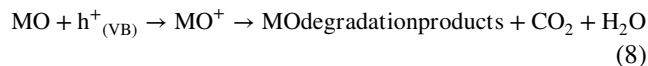
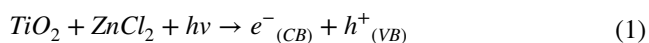
<sup>1</sup> Chemistry Department, Laboratory of Spectroscopy, Molecular Modeling, Materials, Nanomaterials, Water and Environment, CERNE2D, Faculty of Sciences, Mohamed V University in Rabat, 4 Avenue Ibn Battouta BP 1014 RP, Rabat, Morocco

<sup>2</sup> IAV Hassan II, Madinat Al Irfane, B.P. 6202 Rabat, Morocco

## 1 Introduction

Dyes are organic compounds used in many industries: stationary, cosmetics, food, textiles, pharmaceuticals, and in medical diagnostics [1–3]. Water contamination could be due to the color effluents coming from different industries, which is a current problem all over the world [4]. Their removal/pollutant remediation is a major problem because they are highly toxic and non-biodegradable [5, 6]. Advanced Oxidation Processes (POA) for the degradation of organic recalcitrant has been

rapidly developed in the recent years. In addition, the POA driven by sunlight are renewable and ecological in restoration of the environment [7]. Among these POA, photocatalysis has gradually emerged as a promising alternative solution for the removal of soluble organic compounds and it has attracted great interest [8, 9]. It is a fast growing green technology used for the efficient removal of wastewater effluents and the production of ideal hydrogen from water and sunlight [10]. Thus, it offers a great advantage over the other treatment techniques used because it allows the transformation, minimization, and deactivation of persistent compounds in water, as well as the mineralization of all pollutants (bacteria, dyes, organic soils, air pollution ...) while respecting the integrity of the environment and human health [11]. It has extended its application in water treatment due to its potential characteristics such as: feasible operational pressure and temperature, economic reliability and complete degradation of pollutants including parent and intermediate compounds without generating secondary pollutants [12]. Heterogeneous photocatalysis, in the presence of  $\text{TiO}_2$ , is one of the effective photoactive semiconductors that gave better results used in wastewater photodegradation than in the gas phase and also by its potential for application at treatment levels polluted water [8]. The mechanism of this technique is widely studied [13–17], based on the irradiation of the semiconductor by photons of energy greater than or equal to that of its band gap. This absorption results in an activation of the semiconductor. The latter results in the passage of an electron from the valence band to the conduction band, giving rise to an electron/hole pair. These two charge carriers can either recombine by releasing heat or separate to react with species adsorbed on the surface of the semiconductor. Holes in the valence band can oxidize donor molecules (reducing) and react with water molecules to give hydroxyl radicals and electrons can reduce electron acceptors (oxidizing) and react with oxygen species to give superoxide radicals. The reactive oxygen species produced (ROS) interact with contaminants and break them down into less harmful materials [18]. The photocatalytic mechanism is explained by the following equations (Eqs. (1)–(9)).



The use of this technique results in the complete mineralization of these pollutants at room temperature and under atmospheric pressure, while maintaining the integrity of the environment and human health [19, 20].

The use of titanium dioxide for advanced wastewater treatment and water purification processes has attracted growing attention since 1972 [21, 22]. To extend the photoresponse of  $\text{TiO}_2$  to the visible region, many modification methods, such as metal ion doping [23], non-metal doping [24], noble metal deposition [25, 26], composite semiconductors [27, 28], surface dye sensitization [29], and photosensitive material modifications [30], heterojunction with other semiconductors, and copolymerization have been reported. Among these strategies, doping is a suitable and effective technique to modulate the band gap, reduce the high interlayer resistance, differentiate the reaction sites for reduction and oxidation reactions, and improve the photocatalytic activity of  $\text{TiO}_2$  for water purification. Doping has been a “rising star” technique to overcome the limitations offered by pristine photocatalysts [31].

Furthermore, elemental doping is considered a versatile strategy and capable of tailoring the band gap, promoting a targeted application via incorporation of cations, anions or codoping. Due to doping, the absorbed light can be easily converted into charge carriers and ultimately into reactive species [31].

The aim of this work is to study the adsorption and photodegradation of methyl orange dye in an aqueous medium in the presence of pure and doped  $\text{TiO}_2$  Sachtopore nanoparticles, using different percentages of zinc ( $\text{ZnCl}_2$ ) synthesized by the coprecipitation method, and  $\text{TiO}_2$  Degussa P25 was used as reference, because of its high purity and wide use in industrial applications and in scientific research [32].

## 2 Materials and methods

### 2.1 Reactants

Methyl orange is an anionic dye and classified among the azo dyes which are the most frequently used by the textile industries, because of their high dyeing power on several fibers on the one hand and their thermodynamic stability

on the other (Fig. 1). However, the choice of MO dye is their hydrophobic property and the solubility in effluents, which makes methyl orange one of the major pollutants of liquid discharges of textiles dyeing [33]. In addition, this dye, which has been widely used to simulate organic pollutants in wastewater in laboratories [34–36], has been chosen as a pollutant in our work.

The photocatalytic degradation was carried out using  $\text{TiO}_2$  photocatalysts for comparison:  $\text{TiO}_2$  P25,  $\text{TiO}_2$  Sachtopore,  $\text{TiO}_2$  Sachtopore ( $\text{ZnCl}_2/\text{TiO}_2=0.1\%$ ),  $\text{TiO}_2$  Sachtopore ( $\text{ZnCl}_2/\text{TiO}_2=0.2\%$ ).

## 2.2 Synthesis of Zn-doped $\text{TiO}_2$

$\text{TiO}_2$  Sachtopore was purchased without further purification. This source was evaluated without further processing. The co-precipitation process was used to prepare powders of different weight percent  $\text{ZnCl}_2/\text{TiO}_2$  ratio = 0.1% and 0.2% based on  $\text{TiO}_2$  Sachtopore semiconductor nanoparticles.  $\text{TiO}_2$  and  $\text{ZnCl}_2$  were weighed in an appropriate amount and dissolved in a solution of hydrochloric acid (HCl). The mixture was put into a sonicator for 2 h to ensure dissolution. To adjust the pH, NaOH was added to the solution. NaOH acts as a co-precipitant. Afterwards, the solution was filtered and the precipitate was obtained, washed and dried at 50 °C in an oven. At the end, grinding photocatalysts synthesized with a mortar and then calcined at 500° C.

## 2.3 Photoreactor and light source

The photocatalytic reactor consists of a pyrex beaker, of a capacity equal to 250 mL. The beaker containing the aqueous solution of the dye and the semiconductor was placed in the reactor away from daylight. UV irradiations are provided from four lamps of 15 W.

## 2.4 Procedure

In the last few decades, several photocatalysts have been developed to address the challenges of water pollution, such

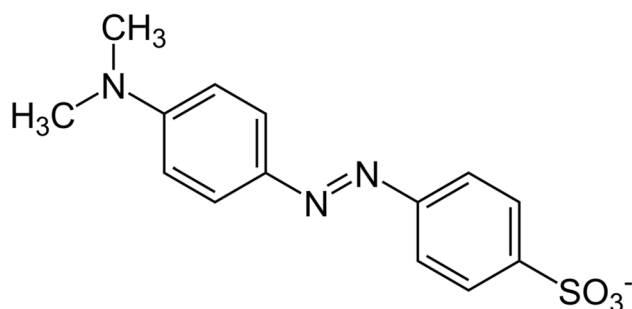


Fig. 1 The orange methyl structure

as  $\text{TiO}_2$ ,  $\text{CuS}_2$ ,  $\text{ZnO}$ , and  $\text{MoS}_2$ . Among these photocatalysts,  $\text{TiO}_2$  is of particular interest because of its crystallographic, electronic and optical properties [37] intro as well as it is a material that simultaneously combines adsorption and photocatalysis.  $\text{TiO}_2$  plays the role of adsorbent in the first place, by fixing on its surface ions or molecules (gases, metals, organic molecules...) in a more or less reversible way. There is a transfer of matter from the aqueous or gaseous phase to the solid surface. Once the  $\text{TiO}_2$  is saturated, it starts to play the role of a photocatalyst after irradiation, where it degrades the pollutants. This represents a practical and low cost advantage.

A volume of known aqueous methyl orange solution (5 mg/L or 10 mg/L) was introduced into the beaker and then into the photoreactor at pH = 5.8 in the presence of (0.2 g/L or 1 g/L)  $\text{TiO}_2$  semiconductor (as a suspended powder). Then, the solution was stirred in the dark for 40 min (until equilibrium adsorption of methyl orange on the catalyst surface was reached). Adsorption is a very important step for our experiment. Then, the lamps were turned on and photocatalytic degradation began for 120 min. Regular samples every 10 min were taken, then filtered through the micro-filter (Millipore type) (0.2  $\mu\text{m}$  porosity) to remove any catalyst particles in suspension, and finally the samples are analyzed through a UV–visible spectrophotometer, which allows direct measurement of the optical densities corresponding to the maximum absorption wavelength of the dye (464 nm).

## 2.5 Characterization

The micrographs of the prepared powders were obtained by transmission electron microscopy (TEM) using Tecnai G2 120 kV and the Bruker AXS D-8 diffractometer was used to identify the morphology of  $\text{TiO}_2$  samples. The Lambda 950 UV–vis-NIR spectrophotometer (Perkin-Elmer) allowed us to record the transmission spectra of  $\text{TiO}_2$  suspensions. For the morphological analysis of  $\text{TiO}_2$  powders, it was performed by scanning electron microscopy (SEM) JEOL JFC-2300HR JEOL JSM-IT 100 with an accelerating voltage of 20 kV. The samples were filtered through a 0.2  $\mu\text{m}$  Millipore membrane. Absorbance measurements were performed using the Mapada 1600 UV/Visible spectrophotometer. The maximum absorption wavelength of methyl orange ( $\lambda_{\text{max}}$ ) is 464 nm [38].

## 3 Results and discussion

### 3.1 Analysis of nanoparticles with transmission electron microscopy (TEM)

Information such as morphology, size distribution, and the chemical contrast in the nanoparticles could be deduced from micrographs of electron microscopy [39]. Figure 2

**Fig. 2** TEM pictures of samples **A** TiO<sub>2</sub> P25, **B** pure TiO<sub>2</sub> Sachtopore, **C** doped TiO<sub>2</sub> Sachtopore (ZnCl<sub>2</sub>/TiO<sub>2</sub>=0.1%), **D** doped TiO<sub>2</sub> Sachtopore (ZnCl<sub>2</sub>/TiO<sub>2</sub>=0.2%)

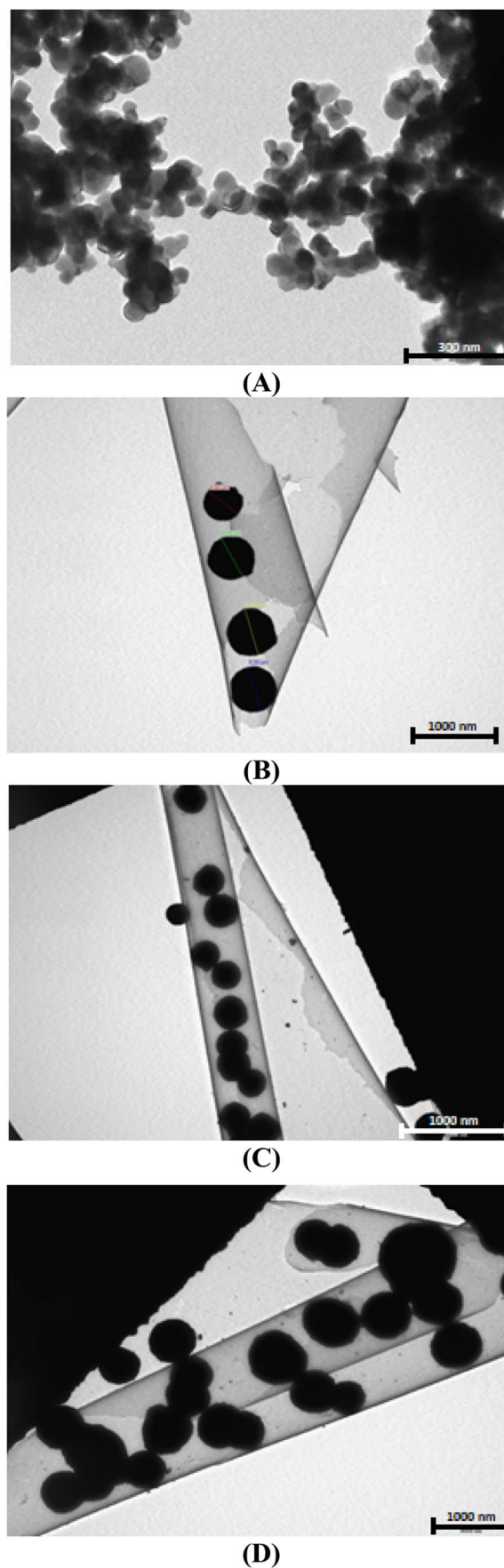
illustrates the micrograph of TiO<sub>2</sub> P25 (A), which shows a mixture of dark and gray nanoparticles with a uniform distribution with a spherical morphology and a heavy agglomeration. Pure TiO<sub>2</sub> Sachtopore (B) shows clearly regular nanoparticles and spherical dark. The micrographs of doped TiO<sub>2</sub> with Zn (C) and (D) show nanoparticles that are fine, dispersed, and of different sizes.

### 3.2 X-ray diffraction nanoparticles characterization (XRD)

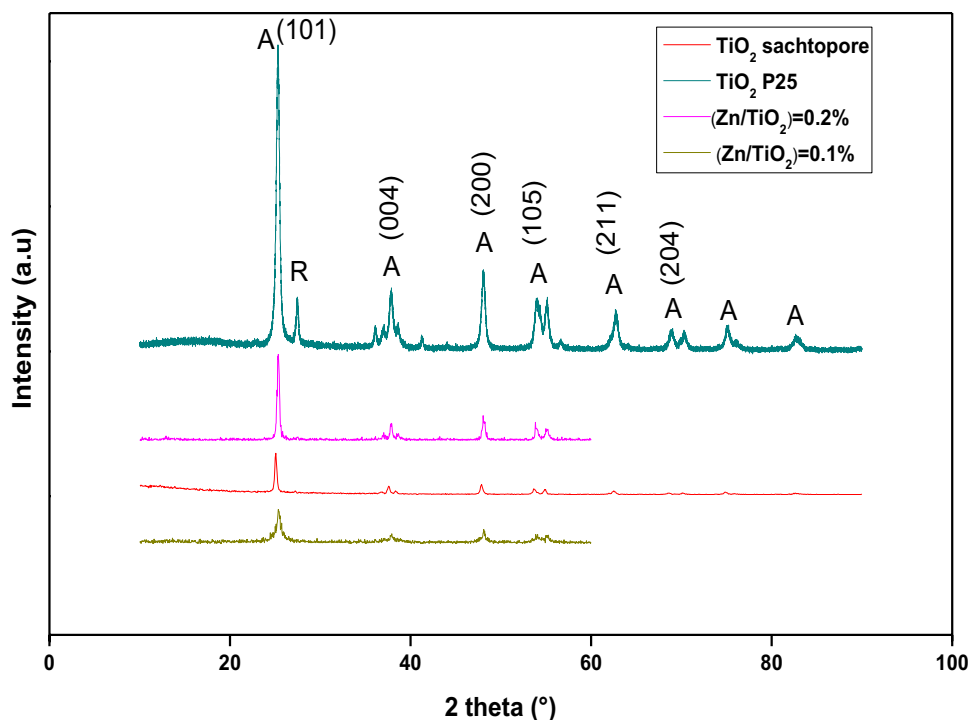
The crystalline structure of samples was studied using X-ray diffraction. Figure 3 shows diffractograms of pure and doped TiO<sub>2</sub> powders. By comparing the diffraction peaks of the samples to TiO<sub>2</sub> diffraction references in the anatase and/or rutile phase, we found that the samples are composed only by crystallites of TiO<sub>2</sub>. The crystalline anatase structure is known for its activity in the oxidation of organic pollutants [40], probably due to the large production of hydroxyl radicals of catalysts comparing to rutile [41]. In the case of TiO<sub>2</sub> P25, the crystallites of TiO<sub>2</sub> are in anatase and rutile phases. However, in the case of pure and doped TiO<sub>2</sub> Sachtopore with zinc, the samples showed exclusively the anatase phase. It has been observed that the intensity of the diffraction peaks of the anatase phase gradually decreased with the increasing of Zn content. This could be attributed to the deformation of the crystal lattice. One can also observe for all the samples: the presence of an intense peak can be attributed to crystallites of TiO<sub>2</sub> anatase. Low intensity peaks could be found in the internal structure of TiO<sub>2</sub> or just on the surface. In addition, the maximum intensities become wider; this is probably due to the formation of small TiO<sub>2</sub> crystallites [42].

The absence of peaks characteristic of zinc oxide phases may indicate the high metal dispersion or be due to the low concentration of Zn doping. This could be attributed to the fine dispersion of zinc ions in small amounts in most TiO<sub>2</sub> nanopowders. We found that there is no appearance of crystallinity difference between doped and undoped TiO<sub>2</sub>. In addition, no significant characteristic zinc peak was found in the doped TiO<sub>2</sub>, also due to the lower amount of zinc.

All Sachtopore samples show similar patterns well attributed to the anatase crystal phase of TiO<sub>2</sub> and there is no other phase in the Sachtopore samples. In each pattern, the six peaks located at angles 2θ: 25.18, 37.84, 48.37, 53.91, 55.02, and 62.65 were observed. These peaks correspond to the (101), (004), (200), (105), (211), and (204) diffraction planes of the anatase phase. The index was made using (JCPDCS card 21–1272).





**Fig. 3** Diffractograms of TiO<sub>2</sub> samples**Table 1** The crystallite size values calculated on the basis of the Debye–Scherrer equation

| Catalysts                   | Size of crystallites (nm) |
|-----------------------------|---------------------------|
| TiO <sub>2</sub> Sachtopore | 49 nm                     |
| (Zn/TiO <sub>2</sub> )=0.1% | 66 nm                     |
| (Zn/TiO <sub>2</sub> )=0.2% | 79 nm                     |
| TiO <sub>2</sub> P25        | 63 nm                     |

From the experiments carried out in XRD, we calculated the crystallite's size of the samples using the Debye–Scherrer relation. The results of the average sizes of the various samples are put together in Table 1. We analyzed the evolution of the crystallite's sizes as a function of the zinc content. It is noted that the size of the nanoparticles of the doped TiO<sub>2</sub> is bigger compared to the TiO<sub>2</sub> P25. Thus, doping has a great influence on the size of the nanoparticles of pure Sachtopore TiO<sub>2</sub>. The higher the Zinc content is, the greater the size of the crystallites become.

### 3.3 Diffuse reflectance spectroscopy study (DRS)

The transmittance of light of different TiO<sub>2</sub> nanoparticles was measured by diffuse reflectance spectroscopy (DRS) (Fig. 4). From Fig. 4, the samples exhibit the same behavior. The spectra of these samples show an absorption edge around 800 nm, meaning that photons with wavelengths below 800 nm (more energy) will be absorbed by these

samples. The threshold for absorption of the samples is related to the presence of TiO<sub>2</sub> and Zn- TiO<sub>2</sub>.

The absorbance curves clearly show the influence of the crystalline phase on the position threshold of the absorption of TiO<sub>2</sub>. In particular, we find that the results of the literature put the optical gap of anatase at 3.2 eV and the rutile at a lower energy, at 3.0 eV, but both in the UV region [43]. In order to determine the optical gap of these samples, the graphical method from the Tauc equations has been used [43, 44]. On the other hand, the band gap energies can also be determined based on the Kubelka–Munk theory, where  $F(R) = (1-R)^2/2R = \alpha$  [45]. Plotting the  $(F(R\infty) \cdot h\nu)^{1/2}$  plot as a function of  $(h\nu)$  allows the value of the band gap energy to be determined by extrapolating the linear portion of the curve to the x-axis. For more clarity, the plots are shown in Fig. 5 and the bandgap values are summarized in Table 2. The band gap values of all photocatalysts were between the values found in the literature for the anatase and rutile phases [46].

The absorption data obtained by DRS allow the nanoparticles to divide into two types. TiO<sub>2</sub> P25 has an absorption threshold in the UV which corresponds to the absorption threshold of TiO<sub>2</sub> in rutile and anatase phases. While the pure TiO<sub>2</sub> Sachtopore, Zn- TiO<sub>2</sub> absorb the energies corresponding to the absorption threshold of TiO<sub>2</sub> in the anatase phase. The absorption in this area is related to the superposition of the energy levels of dopants, which are located between the valence band and the conduction one for TiO<sub>2</sub>. Namely that the dopants could create a level between the

**Fig. 4** Transmittance spectra of TiO<sub>2</sub> samples

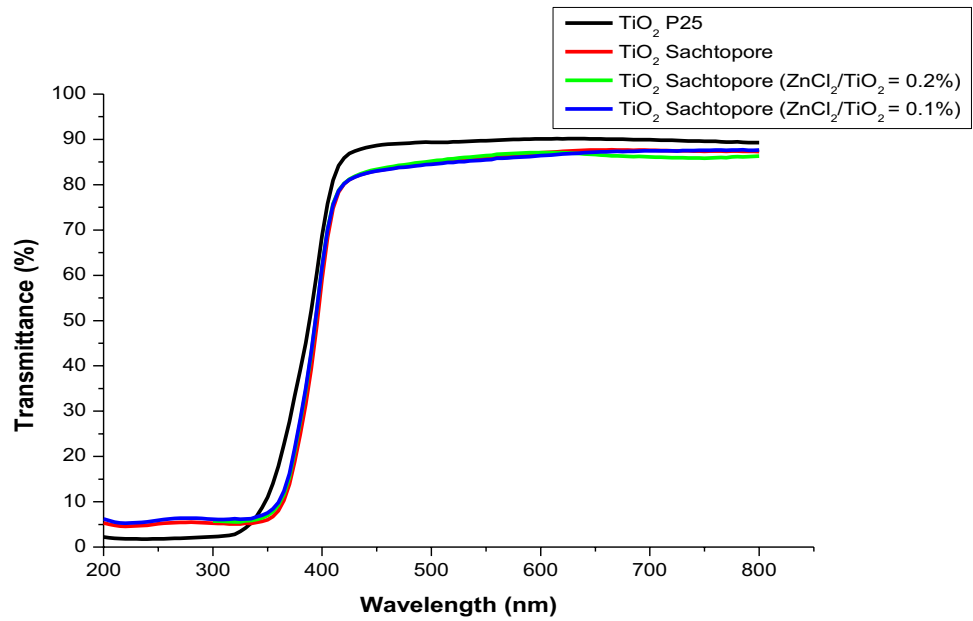


**Fig. 5** Modified curves  $(\hbar\alpha)^{1/2}$  of  $\alpha$  absorbance of different titanium dioxide powders, according to the energy of the incident photon  $\hbar\nu$

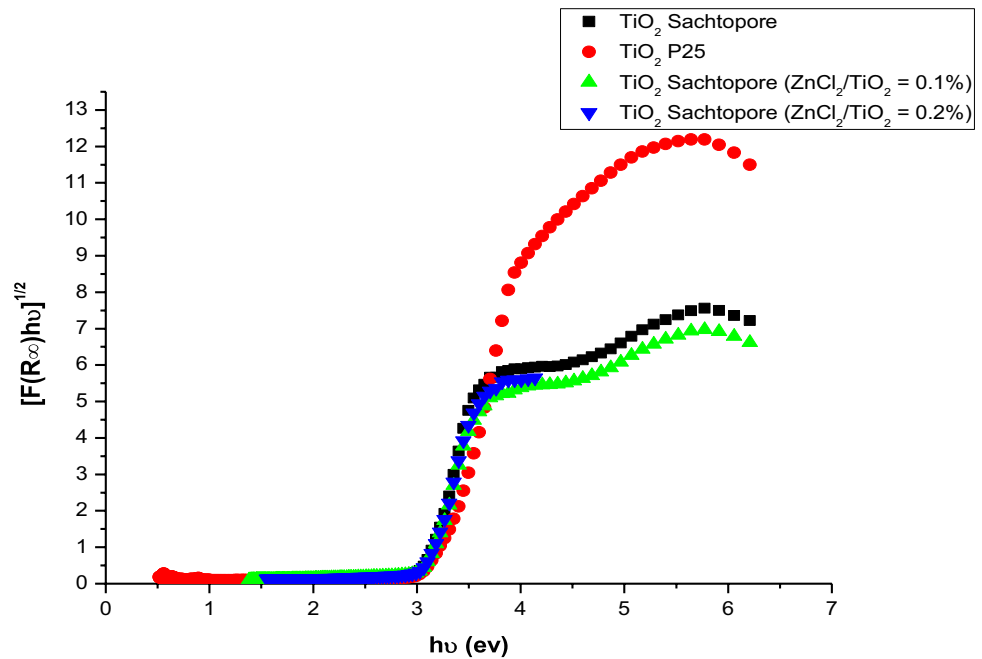


**Table 2** The optical gaps of pure and doped TiO<sub>2</sub> Sachtopore and TiO<sub>2</sub> P25

| Catalysts | TiO <sub>2</sub> Sachtopore pure | TiO <sub>2</sub> Sachtopore doped (ZnCl <sub>2</sub> / TiO <sub>2</sub> = 0.1%) | TiO <sub>2</sub> Sachtopore doped (ZnCl <sub>2</sub> / TiO <sub>2</sub> = 0.2%) | TiO <sub>2</sub> P25 |
|-----------|----------------------------------|---|---|----------------------|
| Gap/ev    | 3.18                             | 3.14  | 3.10  | 3.3                  |

valence and conduction bands and decrease the forbidden band. This allows a small amount of dopants to be inserted into the TiO<sub>2</sub> network and the level of dopants has appeared between the valence band and the TiO<sub>2</sub> conduction band [47].

From the results, we can say that there is a small decrease in the energy gap values for all the catalysts.

### 3.4 SEM images and EDS analysis

SEM images of pure and doped  $\text{TiO}_2$  sachtopore nanoparticles show almost the same, all grains are spherical, dark

and light. The particles are assembled and agglomerated and they are homogeneous. So, we can say that the morphology of  $\text{TiO}_2$  did not change after doping. EDS spectroscopy was used to show the presence of zinc. From the EDS

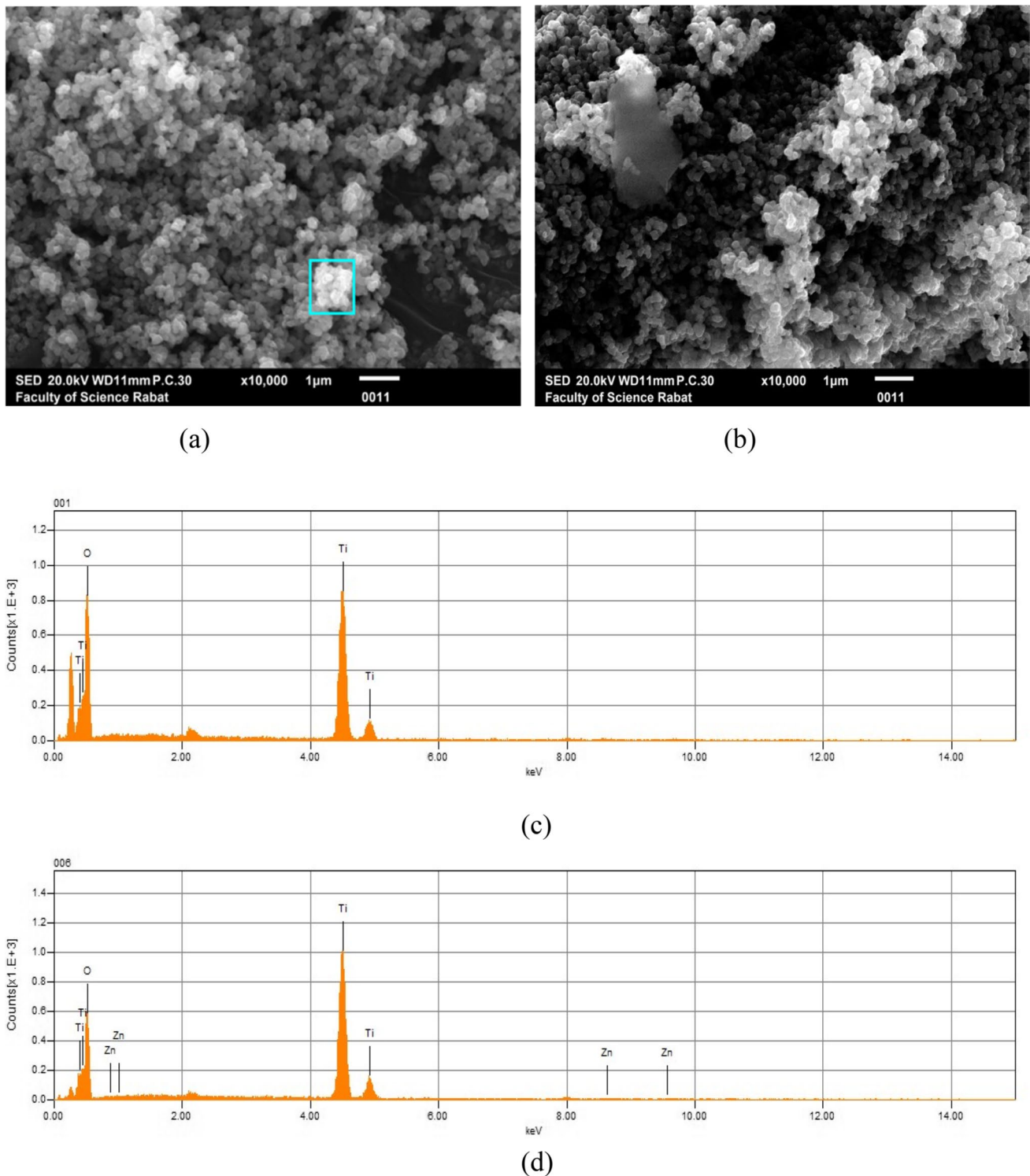


**Fig. 6** SEM images of powders (a)  $\text{TiO}_2$  Sachtopore, (b)  $\text{TiO}_2$  Sachtopore ( $\text{ZnCl}_2/\text{TiO}_2=0.1\%$ ), EDS spectra for (c)  $\text{TiO}_2$  Sachtopore, (d)  $\text{TiO}_2$  Sachtopore ( $\text{ZnCl}_2/\text{TiO}_2=0.1\%$ )

spectrometer of pure Sachtopore  $\text{TiO}_2$ , titanium and oxygen atoms are observed, which shows that the powder contains a quantity of titanium and oxygen (Fig. 6). For zinc-doped  $\text{TiO}_2$ , the same thing is observed but with Zn peaks, so the powder contains titanium and oxygen as well as zinc; these peaks show that the Zn dopant is homogeneously distributed in the  $\text{TiO}_2$  matrix and indicate the presence of the  $\text{ZnCl}_2$  component. The EDS results confirm the doping of sachtopore  $\text{TiO}_2$  with zinc.

### 3.5 Adsorption of methyl orange on different $\text{TiO}_2$ catalysts

The adsorption on the catalyst surface is an initial and essential step for the photocatalytic reaction [48, 49]. In order to identify the optimal conditions for dye degradation, we first started by studying the adsorption of MO on different  $\text{TiO}_2$  catalysts.

### 3.6 Kinetics of methyl orange adsorption on different $\text{TiO}_2$ catalysts

This study aims to verify the adsorption of methyl orange on  $\text{TiO}_2$  catalysts and to compare their efficiencies and to determine the necessary time to achieve the adsorption equilibrium state [50]. Monitoring of adsorption kinetics was performed in darkness under continuous stirring for 2 h (120 min) and the results obtained are grouped in Fig. 7. Regardless of the catalyst, the curves show that the amount adsorbed increases with increasing agitation time and tends toward a limit value corresponding to the maximum amount after about 40 min. This time indicates that the adsorption equilibrium is reached. It is therefore imperative to let the mixture agitate for at least this amount of time prior to irradiation of the mixture. From a kinetics point of view, the adsorption occurs in two steps: the first is quick and the second is slower. It has been observed that over 95% of the

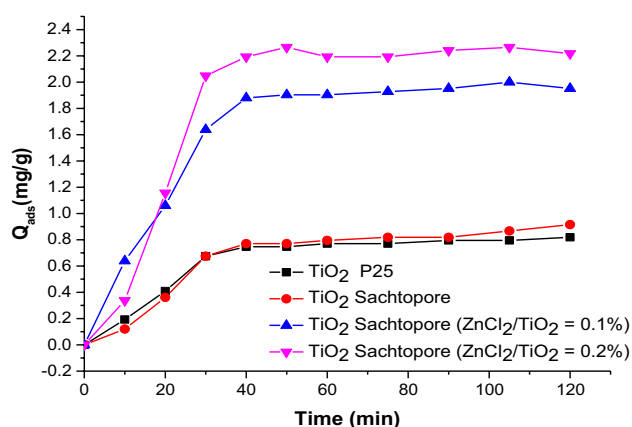


**Fig. 7** Kinetic adsorption of methyl orange (0.5 g/L) on different studied catalysts (10 ppm)

limiting adsorption capacities of catalysts were reached after 30 min of agitation. Beyond this time, the adsorption rate becomes slower. The curves in this figure show that under the same conditions, the dye does not have the same affinity for the solid. Dye adsorbs well on doped  $\text{TiO}_2$  nanoparticles than pure  $\text{TiO}_2$ . In addition, the adsorption capacity depends on the amount of dopant. The amounts of the dye adsorbed on the catalysts equilibrium varies in the following order: doped  $\text{TiO}_2$  Sachtopore ( $\text{ZnCl}_2/\text{TiO}_2 = 0.2\%$ ) > doped  $\text{TiO}_2$  Sachtopore ( $\text{ZnCl}_2/\text{TiO}_2 = 0.1\%$ ) > Pure  $\text{TiO}_2$  Sachtopore >  $\text{TiO}_2$  P25. This improved result can be justified by the increase of the adsorption sites of the catalyst or it could be due to the structure of each catalyst [50].

### 3.7 Methyl orange photodegradation in the presence of the various catalysts

The objective of this part of the work is to study the influence of several parameters such as the concentration of methyl orange, the concentration and the nature of the catalyst, as well as the doping of the catalyst on the degradation kinetics of the methyl orange dye in the presence of different pure and doped  $\text{TiO}_2$  nanoparticles, in aqueous medium. Different  $\text{TiO}_2$  catalysts are used to compare their photocatalytic efficiencies. This study is very important in the design and optimization of industrial systems.

#### 3.7.1 The effect of initial concentration of methyl orange on the kinetics of degradation

The kinetic study of the photocatalytic reaction of methyl orange depending on initial concentration of MO was conducted for two different concentrations of 5 mg/L and

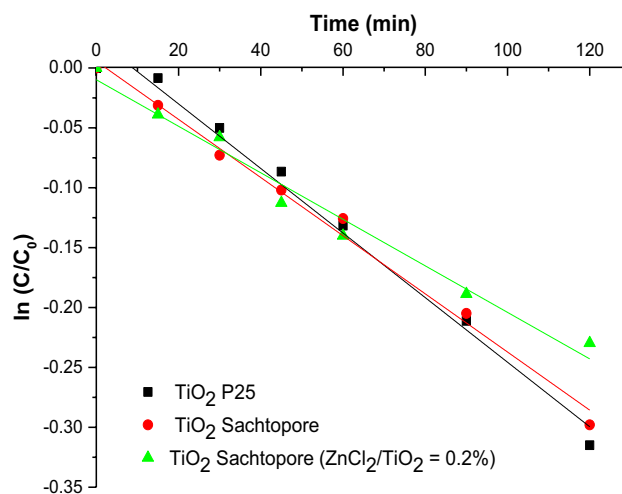


**Fig. 8** Curves of  $\ln(C/C_0)$  in function of irradiation time of MO degradation (10 ppm) in the presence of  $\text{TiO}_2$  (1 g/L)



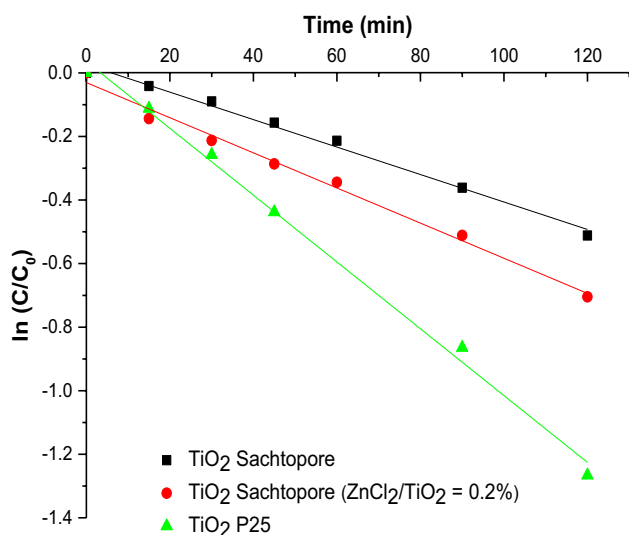


**Fig. 9** Curves of  $\ln(C/C_0)$  in function of irradiation time of MO degradation (5 ppm) in the presence of  $\text{TiO}_2$  (1 g/L)

10 mg/L. Figure 8 and Fig. 9 show the photodegradation kinetics of methyl orange and  $\text{TiO}_2$  (1 g/L). The kinetics of degradation depends on the methyl orange concentration and the nature of the catalyst. The decrease of the degradation of the dye during a high concentration of the latter is explained by the increase of the organic molecules of this pollutant with a number of oxidants generated which is fixed in the solution, all this leads to a low percentage of degradation [51]. On the other hand, perhaps, this is due to the coverage of the photocatalytic sites by the molecules of the dye and decrease in the generation of the oxidizing radicals on the surface of the catalyst [52].

So, the lower the initial concentration of methyl orange is, the higher and faster the degradation will be.

On the other hand, the higher the initial concentration of the dye, the lower the trajectory of the photons entering the solution, which influences the degradation efficiency [53].

The linearity of the curves of  $\ln(C/C_0)$  as a function of time indicates that the degradation follows an apparent first-order ( $\ln(C/C_0) = -K \cdot t$ ). The value of the kinetics constant and the half-life time are shown in Table 3. It was clearly observed that the lower the initial concentration of MO

is, the higher the rate constant increases and the half-life decreases for different  $\text{TiO}_2$  catalysts.

### 3.7.2 The effect of initial concentration of $\text{TiO}_2$ on the degradation kinetics

In heterogeneous catalysis, the reaction rate depends generally on the quantity of the catalyst. In contrast, in the photocatalytic performance, only the  $\text{TiO}_2$  grains that are directly exposed to the radiation are active. It is obvious that the mass needed depends strongly not only on the geometry of the reactor volume, but also on the form in which the photocatalyst is used [54]. The experiments were carried out using two different concentrations 0.2 g/L and 1 g/L of  $\text{TiO}_2$  and the initial concentration of methyl orange used was 10 ppm.

The obtained results (Fig. 10 and Fig. 11) show that when the concentration of  $\text{TiO}_2$  increases, the degradation kinetics increase and the time to remove MO decreases. Indeed, for  $\text{TiO}_2$  concentration of 1 g/L, the photo-disappearance is much more important than for a  $\text{TiO}_2$  concentration of 0.2 g/L. This study showed that a concentration of 1 g/L  $\text{TiO}_2$  for all samples is the optimum concentration. The rate constant varies similarly with the catalyst concentration between 0.2 g/L and 1 g/L (Table 4), which allow us to

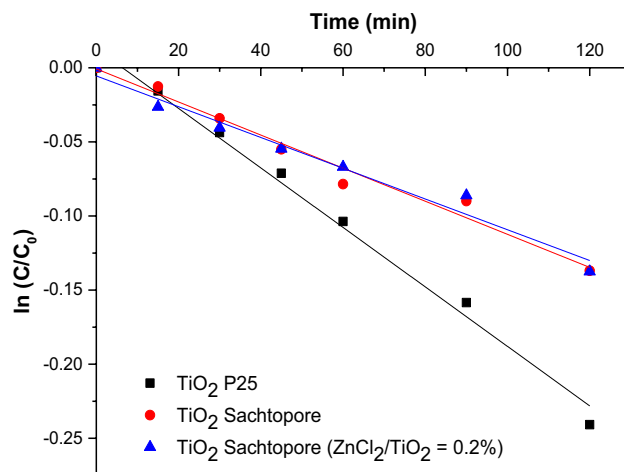


**Fig. 10** Plotting of  $\ln(C/C_0)$  in function of irradiation time of MO degradation (10 ppm) in the presence of  $\text{TiO}_2$  (0.2 g/L)

**Table 3** Kinetic parameters of  $\text{TiO}_2$  (1 g/L) and 10 ppm, 5 ppm of MO and the correlation coefficient  $R^2$

|   | $K_{app}$ ( $\text{min}^{-1}$ )<br>MO (10 ppm) | $K_{app}$ ( $\text{min}^{-1}$ )<br>MO (5 ppm) | $t_{1/2}$ (min)<br>MO (10 ppm) | $t_{1/2}$ (min)<br>MO (5 ppm) | $R^2$<br>MO (10 ppm) | $R^2$<br>MO (5 ppm) |
|---|--|---|--------------------------------|-------------------------------|----------------------|---------------------|
| $\text{TiO}_2$ P25  | 0.0027   | 0.0105  | 257                            | 66                            | 0.9857               | 0.9953              |
| Pure $\text{TiO}_2$ Sachtopore  | 0.0024   | 0.0043  | 289                            | 161                           | 0.9924               | 0.9912              |
| Doped $\text{TiO}_2$ Sachtopore<br>( $\text{ZnCl}_2/\text{TiO}_2 = 0.2\%$ ) | 0.0019   | 0.0055  | 365                            | 126                           | 0.9802               | 0.9913              |

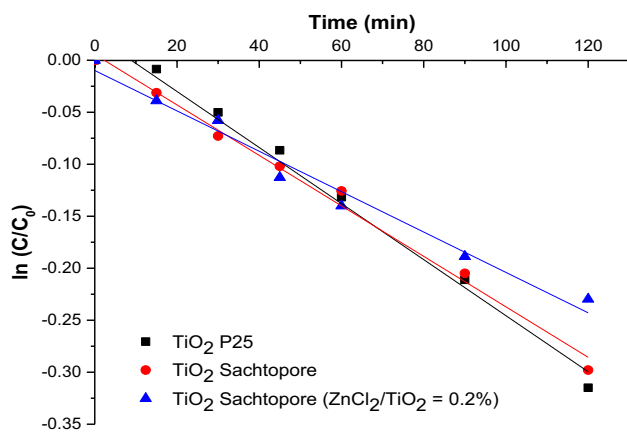


**Fig. 11** Plotting of  $\ln(C/C_0)$  in function of irradiation time of MO degradation (10 ppm) in the presence of  $\text{TiO}_2$  (1 g/L)

predict that all grains are photoactive. The degradation rate is therefore proportional to the mass of  $\text{TiO}_2$  and therefore to the concentration of the adsorbed molecule.

In general, increasing the catalyst concentration promotes the adsorption of the contaminant on the surface. However, for larger quantities, we have noted that degradation kinetics decreases and the reaction rate decreases due to the saturation of the absorption of photons or the loss of light scattering [54]. The linearity of the curves of  $\ln(C/C_0)$  in function of the time indicates that this degradation follows an apparent first-order kinetics. The value of the kinetics constant and the half-life time are summarized in (Table 4). In addition, an increasing on the catalyst concentration promotes the degradation of MO dye. Indeed the half-life time decreased for various catalysts.

### 3.7.3 The effect of catalyst nature on the degradation kinetics

The purpose of this study is to make a comparison between two types of  $\text{TiO}_2$  catalysts (pure  $\text{TiO}_2$  P25 and pure  $\text{TiO}_2$  Sachtopore) in order to assess the effectiveness of the catalyst on the methyl orange degradation kinetics. Methyl orange solution of 5 ppm was introduced into a reactor in

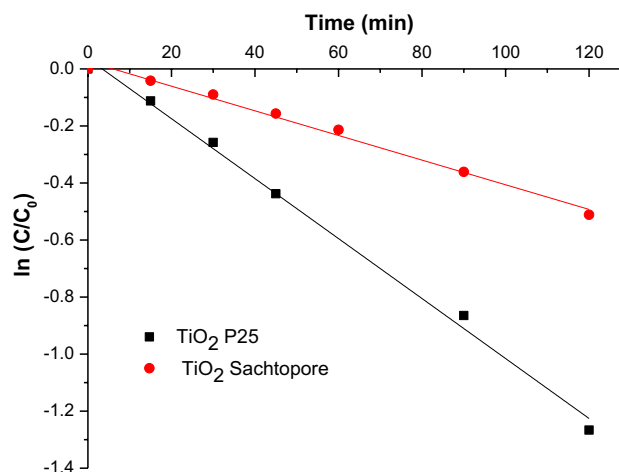


**Fig. 12** Plotting of  $\ln(C/C_0)$  in function of irradiation time of MO degradation (5 ppm) in the presence of  $\text{TiO}_2$  P25, pure  $\text{TiO}_2$  Sachtopore (1 g/L)

the presence of 1 g/L of  $\text{TiO}_2$  (Fig. 12). The photocatalytic efficiency of  $\text{TiO}_2$  depends on the nature of the catalysts used. The linearity  $\ln(C/C_0)$  shows that the degradation kinetics does not change and keeps following the first order (Fig. 12). The values of the rate constant and the half-life time are listed in (Table 5). The photocatalyst  $\text{TiO}_2$  P25 shows greater photocatalytic activity than pure Sachtopore  $\text{TiO}_2$ . This difference in the efficiency may be associated with the difference between textural and structural characteristics of each catalyst. The high performance of  $\text{TiO}_2$  P25 photocatalyst can also be explained by these features (80% anatase and 20% rutile 317  $\text{m}^2/\text{g}$  surface size, nonporous) [54]. Also,  $\text{TiO}_2$  P25 contains anatase crystallites centered by a small rutile core. According to this form, the strong photocatalytic efficiency has been attributed to catalytic “hot spots” at the intersection of the two phases due to the unique surface chemistry [55].

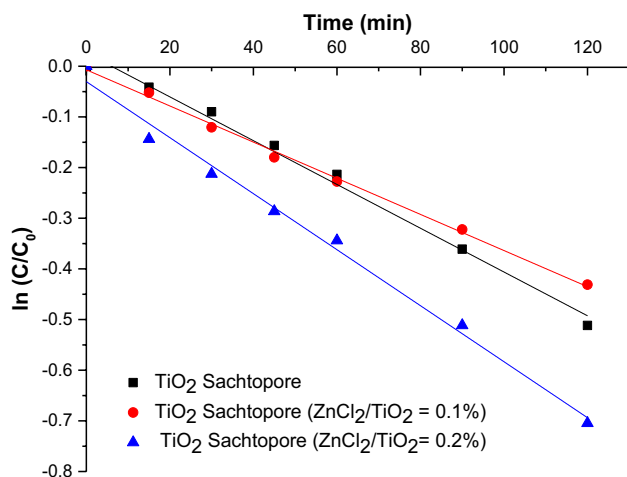
It was clearly observed that the kinetic constant obtained with pure  $\text{TiO}_2$  Sachtopore is smaller than that obtained by  $\text{TiO}_2$  P25, while the half-life time in the presence of  $\text{TiO}_2$  P25 is lower than the one obtained in the presence of pure  $\text{TiO}_2$  sachtopore. This result shows that methyl orange degrades faster in the presence of  $\text{TiO}_2$  P25.

**Table 4** Kinetic parameters of various  $\text{TiO}_2$  catalysts at a concentration of 0.2 g/L and 1 g/L at 10 ppm of MeO and the correlation coefficient  $R^2$

|   | $K_{\text{app}}$ ( $\text{min}^{-1}$ )<br>$\text{TiO}_2$ (0.2 g/L) | $K_{\text{app}}$ ( $\text{min}^{-1}$ )<br>$\text{TiO}_2$ (1 g/L) | $t_{1/2}$ (min)<br>$\text{TiO}_2$ (0.2 g/L) | $t_{1/2}$ (min)<br>$\text{TiO}_2$ (1 g/L) | $R^2$<br>$\text{TiO}_2$ (0.2 g/L) | $R^2$<br>$\text{TiO}_2$ (1 g/L) |
|---|--|--|---|---|-----------------------------------|---------------------------------|
| $\text{TiO}_2$ P25  | 0.0020   | 0.027  | 347   | 257                                       | 0.9889                            | 0.9857                          |
| Pure $\text{TiO}_2$ Sachtopore  | 0.0011   | 0.0024   | 630   | 288                                       | 0.9788                            | 0.9924                          |
| Doped $\text{TiO}_2$ Sachtopore<br>( $\text{ZnCl}_2/\text{TiO}_2 = 0.2\%$ ) | 0.0010   | 0.0019   | 693   | 365                                       | 0.9747                            | 0.9802                          |

**Table 5** Kinetic parameters of TiO<sub>2</sub> and the coefficient of determination R<sup>2</sup>

|                                       | TiO <sub>2</sub> P25 | Pure TiO <sub>2</sub> Sachtopore |
|---------------------------------------|----------------------|----------------------------------|
| K <sub>app</sub> (min <sup>-1</sup> ) | 0.0105               | 0.0043                           |
| t <sub>1/2</sub> (min)                | 66                   | 161                              |
| R <sup>2</sup>                        | 0.9953               | 0.9912                           |

**Fig. 13** Plot of  $\ln(C/C_0)$  versus irradiation time of MO degradation (5 ppm) in the presence of pure and doped TiO<sub>2</sub> Sachtopore (1 g/L)

### 3.7.4 The effect of dopant on the kinetics of degradation

Several important studies have been done on the modification of materials in order to obtain stronger photocatalysts, such as modification or surface formation [56–58] of heterostructures with other substances [59, 60]. Element doping (N, C, Cu, Ag, Nb...) is an available and practical method [61, 62] and effective in improving the photocatalytic yield.

Moreover, doping with alkali metals (Na, K), nonmetals (B, C, N, O, P, S, Cl, and Br, etc.), transition elements (Fe, Cd, Co, Mo, V, etc.), and rare earth metals (Ce, Eu, Se, Y) induces a reduction of the band gap and a shift of the photocatalytic response to the visible region of the solar spectrum [31].

The purpose of this study is to make a comparison between pure TiO<sub>2</sub> Sachtopore and doped with different percentages of zinc chloride (ZnCl<sub>2</sub>) to evaluate the efficiency

**Table 6** Kinetic parameters obtained

|   | K <sub>app</sub> (min <sup>-1</sup> ) | t <sub>1/2</sub> (min) | R <sup>2</sup> |
|---|---------------------------------------|------------------------|----------------|
| Pure TiO <sub>2</sub> Sachtopore  | 0.0043                                | 161                    | 0.9912         |
| Doped TiO <sub>2</sub> Sachtopore (ZnCl <sub>2</sub> /TiO <sub>2</sub> =0.1%) | 0.0036                                | 192                    | 0.9970         |
| Doped TiO <sub>2</sub> Sachtopore (ZnCl <sub>2</sub> /TiO <sub>2</sub> =0.2%) | 0.0055                                | 126                    | 0.9913         |

of the catalyst on the degradation of methyl orange. Methyl orange solution of 5 ppm was introduced into a reactor in the presence of 1 g/L of TiO<sub>2</sub> (Fig. 13).

The curves  $\ln(C/C_0) = f(t)$  show that under the same conditions, MO dye does not exhibit the same affinity for the solid. The photocatalytic degradation efficiency of the catalysts varies in the following descending order: doped TiO<sub>2</sub> Sachtopore (ZnCl<sub>2</sub>/TiO<sub>2</sub>=0.2%) > Pure TiO<sub>2</sub> Sachtopore > doped TiO<sub>2</sub> Sachtopore (ZnCl<sub>2</sub>/TiO<sub>2</sub>=0.1%).

Table 6 groups the values of the half-life time and the speed constant of each catalyst.

Doping improves the photo-reactivity of TiO<sub>2</sub> Sachtopore. Zn<sup>2+</sup> can play both as an electron and a trap hole, which does not leave the recombination of photogenerated e<sup>-</sup> / h<sup>+</sup> pairs on the surface of the semiconductors [66].

In addition, zinc reveals better results with a mass percentage of 0.2%. However, 0.1% of zinc does not improve the photocatalytic performance of TiO<sub>2</sub> Sachtopore.

### 3.8 Recent work on photocatalytic degradation using TiO<sub>2</sub> or Zn doped composites as catalysts.

Several works are interested in the study of photocatalytic degradation using TiO<sub>2</sub> or zinc-doped composites as catalysts in order to remove different pollutants; in this paragraph, we will quote some studies found in the literature in order to have a recent report and also to make a comparison.

We found a study on the degradation of bisphenol S (BPS) by persulfate activation under UV-LED using mixed catalysts: Synergistic effect of Cu-TiO<sub>2</sub> and Zn-TiO<sub>2</sub> for catalysis. They used the sol-gel method to prepare Zn-TiO<sub>2</sub> and Cu-TiO<sub>2</sub>. The two catalysts showed a clear synergistic effect in the photocatalytic degradation process. When the persulfate is 5 mM and the catalyst is 0.3 g/L, the removal rate is 100% in 18 min, in the case of the mixed catalyst (0.2 g/L Zn-TiO<sub>2</sub> and 0.1 g/L Cu-TiO<sub>2</sub>), while in the case of 0.3 g/L Zn-TiO<sub>2</sub> the degradation rate is 58% and 90% in the case of 0.3 g/L Cu-TiO<sub>2</sub>. Several factors were investigated: the Cu-TiO<sub>2</sub>/Zn-TiO<sub>2</sub> ratio, the catalyst dosage, the persulfate dosage, the initial BPS concentration and the initial pH of the solution and the optimal conditions were determined. In summary, in this study, the degradation efficiency of BPS is improved if single metal-doped TiO<sub>2</sub> is replaced by mixed TiO<sub>2</sub>. This technique makes the catalyst more efficient [67].

In another work, the authors developed a solar-derived TiO<sub>2</sub>/g-C<sub>3</sub>N<sub>4</sub> heterostructure photocatalyst without noble

metal by the microwave-assisted hydrothermal route for high photocatalytic activity. The prepared photocatalysts were investigated for photocatalytic hydrogen production and methylene blue dye degradation. 7.5 mg is the weight of the  $\text{TiO}_2/\text{g-C}_3\text{N}_4$  photocatalyst that showed the highest dye degradation removal rate (84.61%) and also a photocatalytic hydrogen productivity of  $110 \mu\text{mol g}^{-1} \text{h}^{-1}$ , which is 2.0 times higher than that of pristine  $\text{TiO}_2$ . This significant increase in hydrogen productivity results from the extended UV–visible light absorption capacity, which increases the charge carrier separation very efficiently. Moreover, they also showed that the enhanced photocatalytic activity is due to the interfacial contact between  $\text{TiO}_2$  and  $\text{g-C}_3\text{N}_4$ , which effectively reduces electron–hole recombination. This technique provides highly efficient photocatalysts for a wide range of applications such as organic dye degradation, hydrogen evolution, and water treatment [68].

There is also another work on photo-induced charge separation at the interface of  $\text{Zn-Pd/TiO}_2$  hybrids for enhanced photocatalytic and electrochemical activity. In this work, the authors used different hybrids to change the role between Ohmic and Schottky barriers to improve the photocatalytic activity. To form hybrids, metal nanoparticles (Pd and Zn) and bimetallic nanoparticles ( $\text{ZnPd}$ ) are opted to study the interface modification by UPS and XPS. The study showed that  $\text{TiO}_2$  nanorods fabricated with Pd and  $\text{ZnPd}$  ( $\text{TiO}_2$  NR) show the constitution of a Schottky barrier with upward band bending at the interface. Thus,  $\text{TiO}_2$  nanorods ( $\text{TiO}_2$  NR) fabricated with Zn show an ohmic barrier with a downward band bend at the interface. At the electrochemical analysis, they analyzed that in  $\text{ZnPd/TiO}_2$  NR, the electrical conductivity is higher, which facilitates the charge carrier transport. Better photocatalytic activity with  $\text{ZnPd/TiO}_2$  NR than with  $\text{Pd/TiO}_2$  NR and  $\text{Zn/TiO}_2$  NR, was due to the improved charge separation at the interface of  $\text{ZnPd/TiO}_2$  NR [69].

## 4 Conclusion

Nowadays, the protection of the environment is a major problem for mankind. The treatment and reuse of industrial water have become an urgent necessity. Methyl orange is one of the most widely used dyes in industries; for this reason, we have been interested in the photocatalytic removal of this dye and have been working on the development of the photocatalytic efficiency of our  $\text{TiO}_2$  Sachtopore catalyst by doping, which is very important in order to obtain a better photo-active solid during degradation.

The photocatalytic degradation of methyl orange was studied using  $\text{TiO}_2$  P25, pure  $\text{TiO}_2$  Sachtopore, and doped  $\text{TiO}_2$  Sachtopore at two different percentages 0.1% and 0.2%. Upon adsorption, the doped  $\text{TiO}_2$  Sachtopore shows a strong adsorption capacity higher than that of  $\text{TiO}_2$  P25. The initial

concentration of methyl orange plays an important role in the photocatalytic degradation kinetics. By decreasing the concentration of methyl orange, the degradation rate increases. Doping also plays an important role in the photocatalytic process and improves the photoreactivity of 0.2%  $\text{TiO}_2$  Sachtopore. The photocatalytic degradation efficiency of the catalysts varies in a decreasing order: for  $\text{TiO}_2$  Sachtopore ( $\text{ZnCl}_2/\text{TiO}_2 = 0.2\%$ ) is 51% > pure  $\text{TiO}_2$  Sachtopore is 36% >  $\text{TiO}_2$  Sachtopore ( $\text{ZnCl}_2/\text{TiO}_2 = 0.1\%$ ) is 32% at a concentration of 5 ppm in the presence of 1 g/L of  $\text{TiO}_2$ .

Furthermore, the photocatalytic degradation depends on the nature and concentration of the catalyst. The degradation of methyl orange follows apparent first order kinetics for all catalysts.

## Declarations

**Conflict of interest** The authors declare no competing interests.

**Life science reporting** No life science threat was practiced in this research.

## References

1. G. Annadurai, R.S. Juang, D.J. Lee, Use of cellulose-based wastes for adsorption of dyes from aqueous solutions. *J. Hazard. Mater.* **92**, 263–274 (2002)
2. P.V. Messina, P.C. Schulz, Adsorption of reactive dyes on titania-silica mesoporous materials. *J. Colloid Interface Sci.* **299**, 305–320 (2006)
3. D. Chakraborty, S. Sen Gupta, Decolourisation of Metanil Yellow by visible-light photocatalysis with N-doped  $\text{TiO}_2$  nanoparticles: influence of system parameters and kinetic study. *Desalin. Water Treat.* **52**, 5528–5540 (2014)
4. P. Niranjana, S. Hrushikesh, M. Sasmita, Decolourization of Methyl Orange using Fenton-like mesoporous  $\text{Fe}_2\text{O}_3\text{-SiO}_2$  composite. *J. Hazard. Mater.* **185**, 359–365 (2011)
5. C.L. Jenkins, Heterogeneous photocatalysis remediation of wastewater polluted by indigoid dyes. *Arch. Environ. Health.* **40**, 7–12 (1978)
6. R.A. Damodar, K. Jagannathan, T. Swaminathan, Decolourization of reactive dyes by thin film immobilized surface photoreactor using solar irradiation. *Sol. Energy.* **81**, 1–7 (2007)
7. S. Patial, P. Raizada, V. Hasija, P. Singh, V.-K. Thakur, V.-H. Nguyen, Recent advances in photocatalytic multivariate metal organic framework (MOFs) based nanostructures toward renewable energy and the removal of environmental pollutants. *Materials Today Energy* **19**, 100589 (2021). <https://doi.org/10.1016/j.mtener.2020.100589>
8. J. Zhang, A. Wei, Q. Wu, D. Zhang, Photocatalytic degradation of Br-trihalomethanes by nanosized  $\text{TiO}_2$ /diatomite hybrid photocatalyst. *Kinetics. Catalys* **57**, 429–433 (2016)
9. A. Garg, V.K. Sangal, P.K. Bajpai, Decolorization and degradation of Reactive Black 5 dye by photocatalysis: modeling, optimization and kinetic study. *Desalin Water Treat* **57**, 1–13 (2016)
10. A. Kumar, P. Raizada, A. Hosseini-Bandegharaei, V. Kumar Thakur, V.-H. Nguyen, P. Singh, C., N-Vacancies defect



- engineering polymeric carbon nitride meeting photocatalysis: viewpoints and challenges. *J Mater Chem A* **9**, 111–153 (2021). <https://doi.org/10.1039/D0TA08384D>
11. B. Regraguy, M. Rahmani, J. Mabrouk, F. Drhimer, I. Ellouzi, C. Mahmoud, A. Dahchour, M. El Mrabet, S. El Hajjaji, Photocatalytic degradation of methyl orange in the presence of nanoparticles NiSO<sub>4</sub>/TiO<sub>2</sub>. *Nanotechnology for Environ. Eng.* **7**, 157–171 (2022). <https://doi.org/10.1007/s41204-021-00206-0>
  12. A. Kumar, P. Raizada, P. Singh, R. Saini, A. Saini, A. Hosseini-Bandegharai, Perspective and status of polymeric graphitic carbon nitride-based Z-scheme photocatalytic systems for sustainable photocatalytic water purification. *Chem. Eng. J.* **391**, 123496 (2020). <https://doi.org/10.1016/j.cej.2019.123496>
  13. M. Nikazar, Kh. Gholivand, K. Mahanpoor, Using TiO<sub>2</sub> supported on clinoptilolite as a catalyst for photocatalytic degradation of Azo Dye Disperse Yellow 23 in water. *Kinet. Catal.* **48**, 214 (2007)
  14. A.V. Vorontsov, D.V. Kozlov, P.G. Smirniotis, V.N. Parmon, TiO<sub>2</sub> Photocatalytic oxidation I Photocatalytic for liquid-phase and gas-phase processes and the photocatalytic for liquid-phase and gas-phase processes and the photocatalytic degradation of chemical warfare agent simulants in a liquid phase. *Kinet. Catal.* **46**, 189 (2005)
  15. D. Zhang, A. Wei, J. Zhang, R. Qiu, The photocatalytic interaction of Cr (VI) ions and phenol on polymer-modified TiO<sub>2</sub> under visible light irradiation. *Kinet. Catal.* **56**, 569–573 (2015)
  16. E.N. Kabachkov, E.N. Kurkin, V.A. Nadochenko, A.A. Terent'ev, Fourier transform infrared spectroscopic study of the photocatalytic degradation of cancerous cells on titanium dioxide. *High Energy Chem* **44**, 426–430 (2010)
  17. D. Zhang, R. Qiu, A. Wei, S. Wang, Influences of organic compounds on the visible light induced photocatalytic reduction of Cr (VI). *Kinet. Catal.* **55**, 793–797 (2014)
  18. I. Bencheikh, K. Azoulay, J. Mabrouki, S. El Hajjaji, A. Dahchour, A. Moufti, D. Dhiba, The adsorptive removal of MB using chemically treated artichoke leaves: parametric, kinetic, isotherm and thermodynamic study. *Scientific African* **9**, e00509 (2020)
  19. M. Sökmen, A. Özkan, Decolourising textile wastewater with modified titania: the effects of inorganic anions on the photocatalysis. *Photochem Photobiol A* **147**, 77–81 (2002)
  20. J. Mabrouki, A. Moufti, I. Bencheikh, K. Azoulay, Y. El Hamdouni, S. El Hajjaji, "Optimization of the coagulant flocculation process for treatment of leachate of the controlled discharge of the City Mohammedia (Morocco)." *International Conference on Advanced Intelligent Systems for Sustainable Development*. Springer, Cham, 2019
  21. B. Lili Zhanga, F. Lva, W. Zhanga, R. Li, Hui Zhonga, Yu. YijiangZhaoa, B.X. Zhanga, Photo degradation of methyl orange by attapulgite–SnO<sub>2</sub>–TiO<sub>2</sub> nanocomposites. *J Hazard Mater* **171**, 294–300 (2009)
  22. K. Azoulay, I. Bencheikh, J. Mabrouki, N. Samghouli, A. Moufti, A. Dahchour, S. El Hajjaji, "Adsorption mechanisms of azo dyes binary mixture onto different raw palm wastes." *International Journal of Environmental Analytical Chemistry*: 1–20 (2021)
  23. T.Z. Tong, J.L. Zhang, B.Z. Tian, F. Chen, D.N. He, Preparation of Fe<sup>3+</sup>-doped TiO<sub>2</sub> catalysts by controlled hydrolysis of titanium alkoxide and study on their photocatalytic activity for methyl orange degradation. *J. Hazard. Mater.* **155**, 572–579 (2008)
  24. J.H. Sun, L.P. Qiao, S.P. Sun, G.L. Wang, Photocatalytic degradation of Orange G on nitrogen-doped TiO<sub>2</sub> catalysts under visible light and sunlight irradiation. *J. Hazard. Mater.* **155**, 312–319 (2008)
  25. I. Bencheikh, K. Azoulay, J. Mabrouki, S. El Hajjaji, A. Moufti, N. Labjar, The use and the performance of chemically treated artichoke leaves for textile industrial effluents treatment. *Chemical Data Collections* **31**, 100597 (2021)
  26. Z.L. Jin, X.J. Zhang, G.X. Lu, S.B. Li, Improved quantum yield for photocatalytic hydrogen generation under visible light irradiation over eosin sensitized TiO<sub>2</sub>—investigation of different noble metal loading. *J. Mol. Catal. A: Chem.* **259**, 275–280 (2006)
  27. Y.J. Zhang, W. Yan, Y. Wu, P. Zhen, H. Wang, Synthesis of TiO<sub>2</sub> nanotubes coupled with CdS nanoparticles and production of hydrogen by photocatalytic water decomposition. *Mater. Lett.* **23**, 3846–3848 (2008)
  28. Y.H. Xu, Z.X. Zeng, The preparation, characterization, and photocatalytic activities of Ce–TiO<sub>2</sub>/SiO<sub>2</sub>. *J. Mol. Catal. A Chem.* **279**, 77–81 (2008)
  29. K.S. Yao, D.Y. Wang, C.Y. Chang, K.W. Weng, L.Y. Yang, S.J. Lee, T.C. Cheng, C.C. Hwang, Photocatalytic disinfection of phytopathogenic bacteria by dyes sensitized TiO<sub>2</sub> thin film activated by visible light. *Surf. Coat. Technol.* **202**, 1329–1332 (2007)
  30. D. Wanga, J. Zhanga, Q. Luob, X. Lib, Y. Duana, J. Anb, Characterization and photocatalytic activity of poly (3-hexylthiophene)-modified TiO<sub>2</sub> for degradation of methyl orange under visible light. *J. Hazard Mater.* **169**, 546–550 (2009)
  31. V. Hasija, P. Raizada, A. Sudhaik, K. Sharma, A. Kumar, P. Singh, S.-B. Jonnalagadda, V.-K. Thakur, Recent advances in noble metal free doped graphitic carbon nitride based nanohybrids for photocatalysis of organic contaminants in water: a review, *Applied Mater. Today* **15**, 494–524 (2019)
  32. X.F. Chen, S.R. Lin, S.C. Kou, Effect of composite photo-catalysts prepared with recycled clay brick sands and nano-TiO<sub>2</sub> on methyl orange and NOX removal. *Constr. Build. Mater.* **171**, 152–160 (2018)
  33. K. Dai, H. Chen, T. Peng, D. Ke, H. Yi, Photocatalytic degradation of methyl orange dye in aqueous suspension of mesoporous titania nanoparticles. *Chemosphere* **69**, 1361–1367 (2007)
  34. M.M. Khan, J. Lee, M.H. Cho, Au@TiO<sub>2</sub> nanocomposites for the catalytic degradation of methyl orange and methylene blue: an electron relay effect. *J. Ind. Eng. Chem.* **20**, 1584–1590 (2014)
  35. X. An, C. Gao, J. Liao, X. Wu, X. Xie, Synthesis of mesoporous N-doped TiO<sub>2</sub>/ ZnAl-layered double oxides nanocomposite for efficient photodegradation of methyl orange. *Mater. Sci. Semicond. Process.* **34**, 162–169 (2015)
  36. D. Ljubas, G. Smoljanic, H. Juretic, Degradation of Methyl Orange and Congo Red dyes by using TiO<sub>2</sub> nanoparticles activated by the solar and the solar-like radiation. *J. Environ. Manage.* **161**, 83–91 (2015)
  37. A.A. Al-Kahtani, S.M. Alshehri, M.U. Naushad, Ruksana, T. Ahamad, Fabrication of highly porous N/S doped carbon embedded with ZnS as highly efficient photocatalyst for degradation of bisphenol. *Int. J. Biol. Macromole.* **121**, 415–423 (2019). <https://doi.org/10.1016/j.ijbiomac.2018.09.199>
  38. J.C. Wanga, J. Rena, H.C. Yao, L. Zhanga, J.S. Wanga, S.Q. Zanga, L.F. Hanb, Z.J. Lia, Synergistic photocatalysis of Cr (VI) reduction and 4-Chlorophenol degradation over hydroxylated α-Fe<sub>2</sub>O<sub>3</sub> under visible light irradiation. *J. Hazard. Mater.* **311**, 11–19 (2016)
  39. L. Truffault, C. Andrezza, C.V. Santilli et, S.H. Pulcinelli, Synthesis of PTSH modified CeO<sub>2</sub> nanoparticles: effect on its structure, optical properties and dispersibility. *J Colloids Surface A: Physicochem Eng Aspects* **426**, 63–69 (2013)
  40. M.J. Hernández Rodríguez, E. Pulido Melián, O. González Díaz, J. Arana, M. Macías, A. González Orive, J.M. Dona Rodríguez, Comparison of supported TiO<sub>2</sub> catalysts in the photocatalytic degradation of NOx. *J Mole Catalys A: Chem* **413**, 56–66 (2016)
  41. Q. Xiang, J. Yu, P.K. Wong, Quantitative characterization of hydroxyl radicals produced by various photocatalysts. *J. Colloid Interface Sci.* **357**, 163–167 (2011)
  42. I. Ellouzi, S. El Hajjaji, M. Harir, P.S. Koplín, D. Robert, L. Laânab, Synergistic effects of C, N, S, Fe-multidoped TiO<sub>2</sub> for photocatalytic degradation of methyl orange dye under UV and visible light irradiations. *J. SN Applied Sciences.* **1**, 930 (2019)



43. H. Tang, K. Prasad, R. Sanjinès, P.E. Schmid, F. Lévy, Electrical and optical properties of TiO<sub>2</sub> anatase thin films. *J. Appl. Phys.* **75**, 20–42 (1994)
44. G. L. Chiarello, D. Paola, and E. Selli, Effect of titanium dioxide crystalline structure on the photocatalytic production of hydrogen. *J. Photochem Photobiol Sci.* “from: 6th Eur Meet Solar Chem Photocatalys: Soc, no. Iii, 2011
45. H. Li, B. Liu, S. Yin, T. Sato, Y. Wang, Visible light-driven photocatalytic activity of oleic acid-coated TiO<sub>2</sub> nanoparticles synthesized from absolute ethanol solution. *Nanoscale. Res. Lett.* **10**, 415 (2015)
46. E. Kordouli, V. Dracopoulos, T. Vaimakis, K. Bourikas, A. Lycourghiotis, C. Kordulis, Comparative study of phase transition and textural changes upon calcination of two commercial titania samples: a pure anatase and a mixed anatase-rutile. *J. Solid. State. Chem.* **232**, 42–49 (2015)
47. I. Ellouzi, L. ELayazi, M. Harir, P. Schmitt-Kopplin, L. Laanab, H. Mountacer, S. El Hajjaji, Synthesis and characterization of C, N, S and Fe modified TiO<sub>2</sub> nanophotocatalyst: efficiency on the degradation of methyl orange and levafix blue. *J. Phys. Chem. News.* **75**, 60–67 (2015)
48. M.A. Hasnat, A. Siddiquey, A. Nuruddin, Comparative photocatalytic studies of degradation of a cationic and an anionic dye. *J. Dyes. Pigments* **66**, 185–188 (2005)
49. Y. Xiaohong, F. Xin, F. Zhang, S. Wang, G. Zhang, Effect of vanadium (IV)-doping on the visible light-induced catalytic activity of titanium dioxide catalysts for methylene blue degradation. *J. Environ. Eng. Sci.* **89**, 149–152 (2006)
50. A. Belmouden, Y. Assabbane, Ait-Ichou, Adsorption characteristics of a phenoxy acetic acid herbicide on activated carbon. *J. Environ. Monit.* **2**, 257–260 (2000)
51. H.B. Hadjltaief, M. Ben Zina, M.E. Galvez, P. Da Costa, Photocatalytic degradation of methyl green dye in aqueous solution over natural clay- supported ZnO–TiO<sub>2</sub> catalysts. *J. Photochem Photobiol A: Chem* **315**, 25–33 (2016)
52. Z. Vaez, V. Javanbakht, Synthesis, characterization and photocatalytic activity of ZSM 5/ZnO nanocomposite modified by Ag nanoparticles for methyl orange degradation, *J. Photochemistry and Photobiology A: Chemistry*. 112064 (2019). <https://doi.org/10.1016/j.jphotochem.2019.112064>
53. N. Chekira, O. Benhabiles, D. Tassalit, N.A. Laoufi, F. Bentahar, Photocatalytic degradation of methylene blue in aqueous suspensions using TiO<sub>2</sub> and ZnO. *J. Desalin. Water Treat.* **57**, 1–7 (2016)
54. A. El Yadini, B. Marouane, A. Ahmido, P. Dunlop, J. Anthony Byrne, M. EL Azzouzi, S. EL Hajjaji, Photolysis and photodegradation of Fenamiphos insecticide by using slurry and supported TiO<sub>2</sub>. *J. Mater. Environ. Sci.* **4**(6), 973–980 (2013)
55. A. El Yadini, H. Saufi, P. S. M. Dunlop, J. Anthony Byrne, M. El Azzouzi, S. El Hajjaji, Supported TiO<sub>2</sub> on borosilicate glass plates for efficient photocatalytic degradation of fenamiphos. *J. of Catalysts.* **8** (2014)
56. W.W. Zhong, Y.F. Lou, S.F. Jin, W.J. Wang, L.W. Guo, A new Bi-based visible-light sensitive photocatalyst BiLa<sub>1.4</sub>Ca<sub>0.6</sub>O<sub>4.2</sub>: crystal structure, optical property and photocatalytic activity. *Sci. Rep.* **6**, 23235–23542 (2016)
57. W.W. Zhong, W.G. Tu, Y. Xu, B.S. Zhan, S.F. Jin, R. Xu, Conductive FeSe nanorods: a novel and efficient co-catalyst deposited on BiVO<sub>4</sub> for enhanced photocatalytic activity under visible light. *J. Environ. Chem. Eng.* **5**, 4206–4211 (2017)
58. M. Ghanbari, M. Salavati, Ti<sub>4</sub>CdI<sub>6</sub> nanostructures: facile sonochemical synthesis and photocatalytic activity for removal of organic dyes. *Inorg. Chem.* **57**, 11443–11455 (2018)
59. A. Abbasi, D. Ghanbari, M. Salavati, M. Hamadianian, Photo-degradation of methylene blue: photocatalyst and magnetic investigation of Fe<sub>2</sub>O<sub>3</sub>-TiO<sub>2</sub> nanoparticles and nanocomposites. *J. Mater. Sci. Mater. Electron.* **27**, 4800–4809 (2016)
60. M. Ghanbari, F. Soofivand, M. Salavati, Simple synthesis and characterization of Ag<sub>2</sub>CdI<sub>4</sub>/AgI nanocomposite as an effective photocatalyst by co-precipitation method. *J. Mol. Liq.* **223**, 21–28 (2016)
61. G.N. Xiao, C.W. Shi, K. Lv, C. Ying, Y.Q. Wang, Nb-doping TiO<sub>2</sub> electron transporting layer for efficient perovskite solar cells. *ACS Appl. Energy Mater.* **1**, 2576–2581 (2018)
62. M.V. Dozzi, A. Candeo, G. Marra, C. D’Andrea, G. Valentini, E. Selli, Effects of photodeposited gold vs platinum nanoparticles on N, F-doped TiO<sub>2</sub> photoactivity: a time-resolved photoluminescence investigation. *J. Phys. Chem. C.* **122**, 14326–14335 (2018)
63. S.H. Chen, S.H. Chan, Y.T. Lin, M.C. Wu, Enhanced power conversion efficiency of perovskite solar cells based on mesoscopic Ag-doped TiO<sub>2</sub> electron transport layer. *Appl. Surf. Sci.* **469**, 18–26 (2019)
64. M. Yıldırım, Characterization of the framework of Cu doped TiO<sub>2</sub> layers: an insight into optical, electrical and photodiode parameters. *J. Alloys Compd.* **773**, 890–904 (2019)
65. P. Wang, C. Jia, J. Li, P. Yang, Ti<sub>3+</sub>-doped TiO<sub>2</sub>(B)/anatase spheres prepared using thioglycolic acid towards super photocatalysis performance. *J. of Alloys and Compounds.* **780**, 660–670 (2019)
66. V. Moradi, M.B.G. Jun, A. Blackburn, R.A. Herring, Significant improvement in visible light photocatalytic activity of Fe doped TiO<sub>2</sub> using an acid treatment process. *J. Appl. Surf. Sci. B.* **427**, 791–799 (2018)
67. Y. Zhang, W. Chu, Bisphenol S degradation via persulfate activation under UV-LED using mixed catalysts: synergistic effect of Cu–TiO<sub>2</sub> and Zn–TiO<sub>2</sub> for catalysis. *Chemosphere* **286**, 131797 (2022)
68. Y.R. Girish, Udayabhanu, G. Alnagar, A. Hezam, M.B. Nayan, G. Nagaraju, K. Byrappa, Facile and rapid synthesis of solar-driven TiO<sub>2</sub>/g-C<sub>3</sub>N<sub>4</sub> heterostructure photocatalysts for enhanced photocatalytic activity. *J. Sci: Adv Mater Device* **7**, 100419 (2022)
69. P. Bamola, S. Rawat, D.K. Pathak, M. Sharma, C. Dwivedi, S. Farsinezhad, R. Kumar, H. Sharma, Photoinduced charge separation at Zn-Pd/TiO<sub>2</sub> hybrids interface for enhanced electrochemical and photocatalytic activity. *J. Phys. D Appl. Phys.* **55**, 335501 (2022). <https://doi.org/10.1088/1361-6463/ac7115>

**Publisher’s note** Springer Nature remains neutral with regard to jurisdictional claims in published maps and institutional affiliations.

Springer Nature or its licensor holds exclusive rights to this article under a publishing agreement with the author(s) or other rightsholder(s); author self-archiving of the accepted manuscript version of this article is solely governed by the terms of such publishing agreement and applicable law.